Internal Dose Assessment of (–)-18F-Flubatine, Comparing Animal Model Datasets of Mice and Piglets with First-in-Human Results

Bernhard Sattler*[1], Mathias Kranz*[1,2], Alexander Starke[3], Stephan Wilke[1], Cornelius K. Donat[3], Winnie Deuther-Conrad[3], Marianne Patt[1], Andreas Schildan[1], Jörg Patt[1], René Smits[4], Alexander Hoepping[4], Peter Schoenknecht[5], Jörg Steinbach[6], Peter Brust*[3], and Osama Sabri*[1]

[1]Department of Nuclear Medicine, University Hospital Leipzig, Leipzig, Germany; [2]Institute of Radiopharmaceutical Cancer Research, Research Site Leipzig, Helmholtz-Zentrum Dresden-Rossendorf, Dresden/Leipzig, Germany; [3]Department of Nuclear Medicine, Diaconal Hospital Henriettenstiftung Hannover, Hannover, Germany; [4]ABX Advanced Biochemical Compounds Ltd., Radeberg, Germany; [5]Department of Psychiatry, University Hospital Leipzig, Leipzig, Germany; and [6]Institute of Radiopharmaceutical Cancer Research, Helmholtz-Zentrum Dresden-Rossendorf, Dresden, Germany

(–)-18F-flubatine is a promising tracer for neuroimaging of nicotinic acetylcholine receptors (nAChRs), subtype α4β2, using PET. Radiation doses after intravenous administration of the tracer in mice and piglets were assessed to determine the organ doses (ODs) and the effective dose (ED) to humans. The results were compared with subsequent clinical investigations in human volunteers. **Methods:** Twenty-seven female CD1 mice (weight ± SD, 28.2 ± 2.1 g) received intravenous injection of 0.75 ± 0.33 MBq of (–)-18F-flubatine. Up to 240 min after injection, 3 animals per time point were sacrificed and the organs harvested, weighed, and counted in a γ counter to determine mass and activity, respectively. Furthermore, whole-body PET scans of 5 female piglets (age ± SD, 44 ± 3 d; weight ± SD, 13.7 ± 1.7 kg) and 3 humans (2 men and 1 woman; age ± SD, 59.6 ± 3.9 y; weight ± SD, 74.3 ± 3.1 kg) were obtained up to 236 min (piglets) and 355 min (humans) after injection of 186.6 ± 7.4 and 353.7 ± 10.2 MBq of (–)-18F-flubatine, respectively, using a PET/CT scanner. The CT was used for delineation of the organs. Exponential curves were fitted to the time–activity-data, and time and mass scales were adapted to the human anatomy. The ODs were calculated using OLINDA/EXM (version 1.0); EDs were calculated with the tissue-weighting factors of ICRP103. **Results:** After the injection of (–)-18F-flubatine, there were no adverse or clinically detectable pharmacologic effects in any of the subjects. The highest activities after injection were found in the kidneys, urinary bladder, and liver. The urinary bladder receives the highest OD in all investigated species, followed by the kidneys and the liver for animals and humans, respectively. On the basis of mouse, piglet, and human kinetic data, the projected human ED of (–)-18F-flubatine was estimated to be 12.5 μSv/MBq in mice, 14.7 ± 0.7 μSv/MBq in piglets, and 23.4 ± 0.4 μSv/MBq in humans. **Conclusion:** As has been demonstrated for other PET radiotracers, preclinical (i.e., animal-derived) dosimetry underestimates the ED to humans, in the current case of (–)-18F-flubatine by 34%–44%.

Neuronal nicotinic acetylcholine receptors (nAChRs) are involved in memory processes and in learning and neuropsychiatric diseases. The degeneration of nAChRs is related to brain disorders like Parkinson disease (1) and schizophrenia (2). Furthermore, a decrease of nAChRs availability is suggested to be a potential indication for patients with a progressive Alzheimer dementia (3). By visualizing nAChRs in vivo, a prediction of the transformation from mild cognitive impairment to Alzheimer dementia might be possible (4). More information on the role of nAChRs in PET imaging of the brain can be found in the supplemental material (available at http://jnm.snmjournals.org).

Although there are 2 existing enantiomers of 18F-flubatine, (−)- and (+)-18F-flubatine, the (−)-derivate was investigated in this study because it showed faster kinetics than those of (+)-18F-flubatine (5). As a regulatory requirement and to ensure the safety and tolerability in the human body, a whole-body (WB) biodistribution and dosimetry study was performed. Determining the estimated internal radiation dosimetry to humans using animal models is essential before permission for clinical testing can be granted (6). Therefore, the study was divided into a preclinical (nonhuman biologic systems, i.e., mouse, piglet) and an early clinical part including the first-in-human data collection. The preclinical part includes the WB dosimetry of 27 mice as well as the first-time (to our knowledge) use of 5 piglets. The clinical part includes 3 healthy volunteers. The aim of this study was to perform a comparison of biodistribution and internal radiation dosimetry by extrapolating animal data to humans and to validate the results by additional investigation in human volunteers. Furthermore, we propose the general conclusion to correct for the underestimation in the translation of preclinical dose estimates for 18F-labeled ligands to humans.
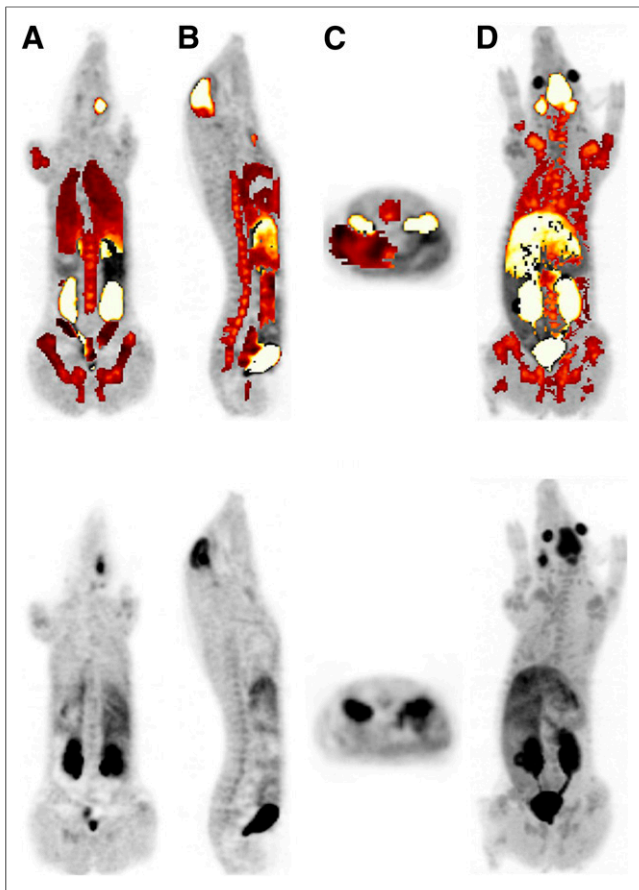
FIGURE 1. Representative PET image (80 min after injection) of piglet, with (top row) and without (bottom row) VOIs superimposed. The figure shows a summary of all investigated organs in piglets from different views: coronal (A), sagittal (B), transversal (liver) (C), and maximum-intensity projection (D) of 1 representative dataset.
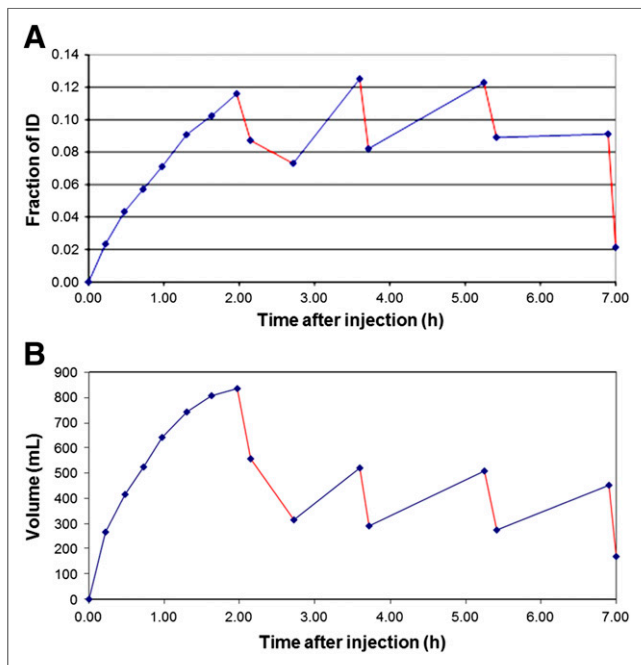

FIGURE 3. Time–activity curve (A) and micturition diagram (B) of urinary bladder (human subject 3).
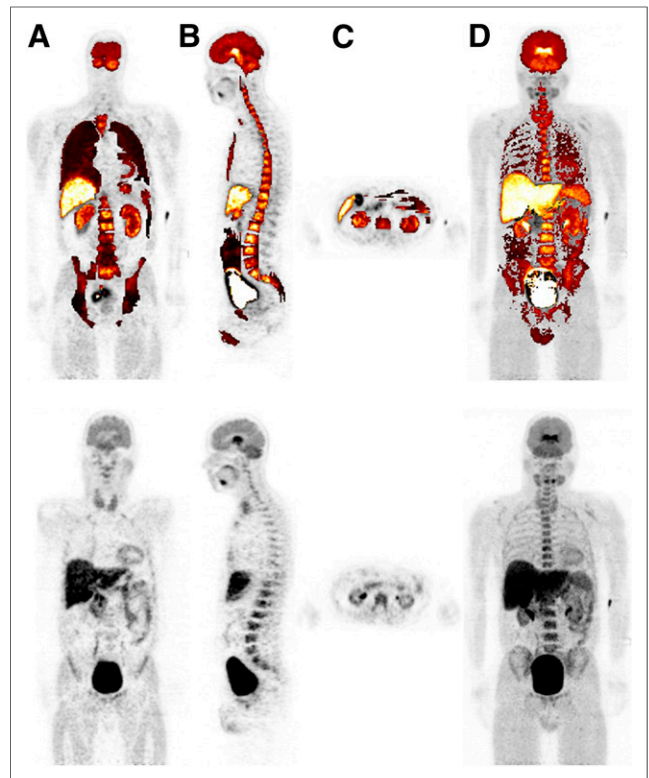

FIGURE 2. Representative PET image (100 min after injection) of human (man), with (top row) and without (bottom row) VOIs highlighted. Different views are shown as coronal (A), sagittal (B), transversal (liver, kidneys) (C), and maximum-intensity projection (D) of 1 representative dataset.

MATERIALS AND METHODS

Synthesis of (−)-^{18}F-Flubatine

A detailed description of the synthesis was published by Deuther-Conrad et al. (*7*) and Patt et al. (*8*), and an improved 2-step strategy was published by Fischer et al. (*4*). Including the 3 healthy volunteers
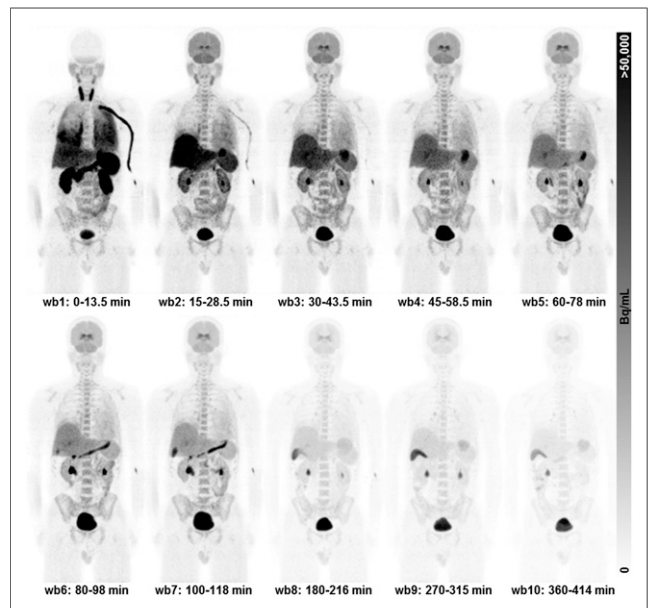

FIGURE 4. Series of human PET scans from injection time until 414 min after injection (maximum-intensity projection).
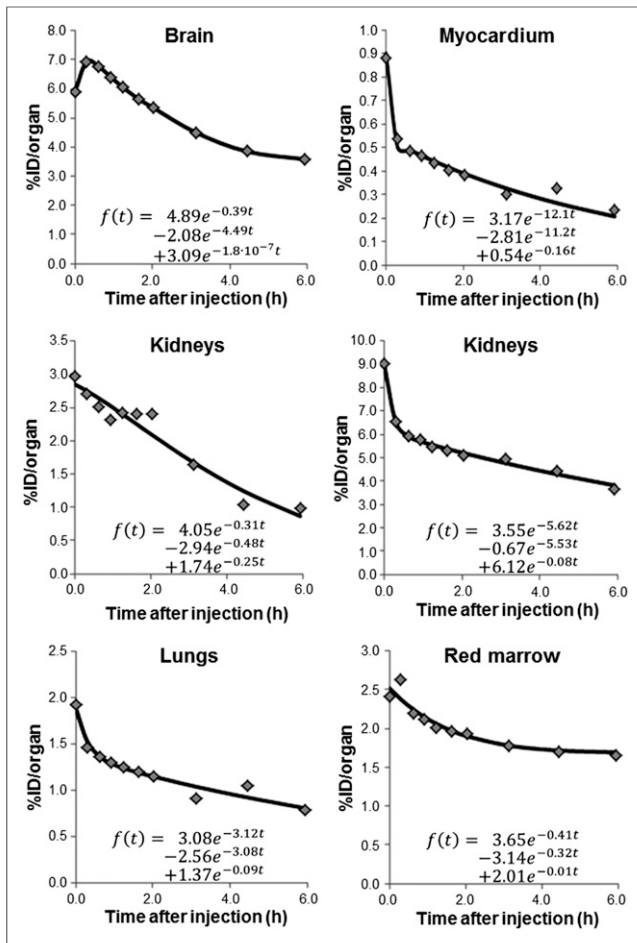
FIGURE 5. Representative $(-)$-^{18}F-flubatine time–activity curves (piglet). To determine number of disintegrations, we used exponential least-mean squared fit. Fit function is shown with the respective curve.

as described in this work, we have injected more than 40 preparations of $(-)$-^{18}F-flubatine in human subjects and had no clinically detectable side effects from the radiopharmaceutical. At the time of injection, the radiopharmaceutical had an injected mass of 0.1 ± 0.08 µg (maximum, 0.4 µg). The use of $(–)$-^{18}F-flubatine was authorized by the responsible authorities in Germany, the Federal Institute for Drugs and Medical Devices (Bundesamt für Arzneimittel und Medizinprodukte, BfArM) and the federal Office for Radiation Protection (Bundesamt für Strahlenschutz, BfS), as well as by the institutional review board (ethics committee).

Preclinical Studies

All experiments involving animals were approved by the respective Institutional Animal Care and Use Committee and are in accordance with national regulations for animal research and laboratory animal care.

Mice. The animals were housed under a 12-h–12-h light–dark cycle and had 2 d for acclimation before the experiments. Twenty-four hours before the investigation, they were fasted while water was still available. Twenty-seven female CD1 mice (weight $\pm$ SD, 28.2 ± 2.1 g) received an intravenous injection of 0.75 ± 0.334 MBq of $(-)$-^{18}F-flubatine with a specific activity greater than 100 GBq/µmol through the tail vein (vena caudata lateralis). At fixed time points, the animals were sacrificed and dissected, and the organs and tissues were harvested and counted in a γ counter to evaluate the activity in each organ.

Piglets. Five female piglets (age $\pm$ SD, 44 ± 3.0 d; weight $\pm$ SD, 13.7 ± 1.7 kg) were anesthetized using ketamine (20 mg/kg), azaperone (2 mg/kg), and 0.5% isoflurane in 70% N_2O/30% O_2, after immobilization with pancuronium bromide (0.2 mg/[kg h] intravenously). All incision sites were infiltrated with 1% lidocaine. The animals were sequentially PET-imaged up to 5 h after intravenous (vena jugularis) injection of 186.6 ± 7.4 MBq of $(-)$-^{18}F-flubatine. The artificial respiration, after surgical tracheotomy, was controlled by a ventilator (Ventilator 710; Siemens-Elema) whereas the existing vein access was used for volume substitution (lactated Ringer solution, 5 mL/[kg h]). The ventilation was set to normoxic and normocapnic blood gas values. To control the arterial blood gas pressure and the acid-base parameters, blood samples from the arteria femoralis with a polyurethane catheter to the aorta abdominalis were manually taken and measured (ABL 50; Radiometer). The body temperature was controlled by an in-ear thermometer and kept at 38°C using an electric blanket. After all preparations for the scan were finished, the concentration of anesthetic gas was reduced to 0.25% isoflurane, 65% N_2O, and 35% O_2.

TABLE 1
ODs and EDs of Mice for $(-)$-^{18}F-Flubatine

Target organ	OD (mSv/MBq)	ED contribution (mSv/MBq)
Adrenals	9.74E−03	8.38E−05
Brain	1.07E−02	1.07E−04
Breasts	5.34E−03	6.41E−04
Gallbladder wall	9.28E−03	7.98E−05
Lower large intestine wall	1.26E−02	7.56E−04
Small intestine	1.30E−02	1.12E−04
Stomach wall	8.51E−03	1.02E−03
Upper large intestine wall	1.07E−02	6.42E−04
Heart wall	7.86E−03	6.76E−05
Kidneys	2.42E−02	2.08E−04
Liver	1.40E−02	5.60E−04
Lungs	8.78E−03	1.05E−03
Muscle	7.07E−03	6.08E−05
Ovaries	1.03E−02	8.24E−04
Pancreas	1.40E−02	1.20E−04
Red marrow	1.09E−02	1.31E−03
Osteogenic cells	1.18E−02	1.18E−04
Skin	4.99E−03	4.99E−05
Spleen	1.15E−02	9.89E−05
Testes	7.84E−03	0.00E+00
Thymus	7.95E−03	6.84E−05
Thyroid	6.46E−03	2.58E−04
Urinary bladder wall	1.04E−01	4.16E−03
Uterus	1.41E−02	1.21E−04
Total body	8.32E−03	0.00E+00
ED (mSv/MBq)		1.25E−02

Mean over 27 subjects; ODs calculated for adult male model (73.7 kg, implemented in OLINDA) based on mouse biodistribution and organ geometry data that were scaled to human circumstances.

TABLE 2
ODs and EDs of Piglets for (−)-^{18}F-Flubatine

Target organ	OD (mSv/MBq)	SD (mSv/MBq)	ED contribution (mSv/MBq)	SD (mSv/MBq)
Adrenals	1.15E−02	8.07E−04	9.89E−05	6.94E−06
Brain	2.78E−02	6.40E−03	2.78E−04	6.40E−05
Breasts	1.68E−02	2.60E−02	2.02E−03	3.11E−03
Gallbladder wall	1.71E−02	2.32E−03	1.47E−04	1.99E−05
Lower large intestine wall	1.10E−02	1.40E−03	6.60E−04	1.69E−04
Small intestine	1.48E−02	2.76E−03	1.27E−04	2.37E−05
Stomach wall	1.27E−02	2.13E−03	1.52Ev03	2.56E−04
Upper large intestine wall	1.54E−02	3.08E−03	9.24E−04	1.85E−04
Heart wall	1.56E−02	2.65E−03	1.34E−04	2.28E−05
Kidneys	4.18E−02	7.29E−03	3.59E−04	6.27E−05
Liver	2.88E−02	8.09E−03	1.15E−03	3.23E−04
Lungs	1.32E−02	1.94E−03	1.58E−03	2.32E−04
Muscle	7.76E−03	7.10E−04	6.67E−05	6.11E−06
Ovaries	1.02E−02	1.17E−03	8.16E−04	9.34E−05
Pancreas	3.39E−02	2.82E−02	2.92E−04	2.42E−04
Red marrow	1.20E−02	1.51E−03	1.44E−03	1.81E−04
Osteogenic cells	1.39E−02	1.46E−03	1.39E−04	1.46E−05
Skin	5.90E−03	5.47E−04	5.90E−05	5.47E−06
Spleen	1.99E−02	4.63E−03	1.71E−04	0.00E+00
Testes	7.36E−03	9.59E−04	0.00E+00	8.25E−06
Thymus	1.85E−02	4.45E−03	1.59E−04	3.83E−05
Thyroid	1.56E−02	5.77E−03	6.24E−04	2.31E−04
Urinary bladder wall	4.55E−02	1.94E−02	1.82E−03	7.76E−04
Uterus	1.14E−02	1.62E−03	9.80E−05	1.39E−05
Total body	9.39E−03	5.20E−04	0.00E+00	0.00E+00
ED (mSv/MBq)			1.47E−02	7.25E−04

Mean over 5 subjects; ODs calculated for adult male model (73.7 kg, implemented in OLINDA) based on piglet biodistribution and organ geometry data that were scaled to human circumstances.

Clinical Study

The institutional review board approved this study, and all subjects signed a written informed consent form. Three healthy volunteers (2 men; age ± SD, 59.6 ± 3.9 y, weight ± SD, 74.3 ± 3.1 kg) were sequentially imaged in a PET/CT system after injection of 353.7 ± 10.2 MBq of (−)-^{18}F-flubatine. At 2, 3.5, 5, and 7 h after injection, the subjects left the PET/CT table, and the urine was collected. The activity excreted in urine was calculated by volume measurement in combination with determination of activity in 1 mL aliquots with a γ counter (Auto-Gamma-Counting System, Cobra II 5003, 7.62-cm [3-in] NaI crystal; Packard).

PET Scan Protocol and Data Acquisition/Evaluation

Data in the 3 species were collected in 2 different ways. Although the harvesting method (6) was chosen for the mice, data acquisition for piglets and humans was applied by sequential, decay-corrected PET imaging on a Siemens Biograph16 PET/CT system (imaging method (6)). The system is a lutetium oxyorthosilicate, 3-dimensional, 41-detector-ring system with an axial field of view of 162 mm, a minimal slice thickness of 2 mm, and a transaxial and axial resolution of 6.5 and 6 mm, respectively. Each sequential and late WB PET scan was preceded by a WB low-dose CT scan for attenuation correction and anatomic orientation.

The piglets were positioned prone with legs alongside the body and the head in a custom-made head-holder. During the dynamic (sequential, without time period between the WB scans) part, 7 WB scans were obtained up to 96 min after injection. The subsequent static part included 3 WB scans (22 min between each WB scan) up to 281 min after injection. Supplemental Table 1 shows the scan protocol used for the PET (Fig. 1) and CT scans of the piglets.

PET imaging in humans was performed with volunteers positioned supine, with their arms alongside their body. The PET frame was acquired using 9 bed positions starting from 1.5 up to 6 min per bed position (Supplemental Table 2), divided into a dynamic and static part. Each of these parts started with a CT scan, at a maximum of 50 mAs and using automated tube current modulation. CT attenuation correction based on low-dose CT transmission data and iterative reconstruction using ordered-subsets expectation maximization (4 iterations and 8 subsets) were applied in both imaged species.

Three mice at each time point (5, 15, 30, 45, 60, 90, 120, 180, and 240 min after injection) were sacrificed and dissected. All relevant

TABLE 3
ODs and EDs of Humans for (−)-^{18}F-Flubatine

Target organ	OD (mSv/MBq)	SD	ED contribution (mSv/MBq)	SD
Adrenals	1.41E−02	6.66E−04	1.22E−04	5.73E−06
Brain	2.76E−02	1.87E−03	2.76E−04	1.87E−05
Breast	7.27E−03	1.36E−04	8.73E−04	1.63E−05
Gallbladder wall	2.78E−02	3.52E−03	2.39E−04	3.02E−05
Lower large intestine wall	1.57E−02	1.85E−03	9.44E−04	1.11E−04
Small intestine	2.56E−02	3.27E−03	2.20E−04	2.81E−05
Stomach wall	2.42E−02	5.80E−03	2.90E−03	6.96E−04
Upper large intestine wall	2.78E−02	3.61E−03	1.67E−03	2.17E−04
Heart wall	1.69E−02	2.38E−03	1.45E−04	2.05E−05
Kidneys	3.86E−02	5.10E−03	3.32E−04	4.39E−05
Liver	4.47E−02	5.47E−03	1.79E−03	2.19E−04
Lungs	3.11E−02	5.37E−03	3.73E−03	6.44E−04
Muscle	8.79E−03	3.41E−04	7.56E−05	2.93E−06
Ovaries	1.31E−02	1.32E−03	1.05E−03	1.06E−04
Pancreas	2.66E−02	3.23E−03	2.29E−04	2.78Ev05
Red marrow	1.91E−02	1.63E−03	2.30E−03	1.95E−04
Osteogenic cells	1.76E−02	6.51Ev04	1.76E−04	6.51E−06
Skin	6.29E−03	2.52E−04	6.29E−05	2.52E−06
Spleen	3.84E−02	1.16E−02	3.30E−04	9.93E−05
Testes	1.54E−02	6.45E−03	1.23E−03	5.16E−04
Thymus	8.76E−03	1.36E−04	7.53E−05	1.17E−06
Thyroid	3.28E−02	1.19E−02	1.31E−03	4.75E−04
Urinary bladder wall	8.02E−02	3.78E−02	3.21E−03	1.51E−03
Uterus	1.49E−02	2.57E−03	1.28E−04	2.21E−05
Total body	1.13E−02	1.00E−04	0.00E+00	0.00E+00
ED (mSv/MBq)			2.34E−02	4.45E−04

Mean over 3 subjects; ODs calculated for adult male model (73.7 kg, implemented in OLINDA) based on human biodistribution and organ geometry data.

organs including the brain, heart, lungs, stomach, small intestine, large intestine, liver, kidneys, urinary bladder, spleen, thymus, pancreas, adrenals, ovaries, blood, skin, muscle, and skeleton were isolated (harvested) and weighed, and their activities were measured in a γ counter. To obtain activity data for muscle and skeleton, an allometric scaling of the weights and volumes using tissue samples was performed (9). The activity data of each organ at the respective time point were subsequently transformed to the percentage injected dose (%ID) using the following equation:

$$\%ID_{organ} = \frac{A_{organ}(t) \times C_{scan}}{A_0(t)}, \qquad \text{Eq. 1}$$

where $A_{organ}(t)$ is the total activity in the respective organ at the corresponding time, C_{scan} the correction factor (supplemental material), and $A_0(t)$ the decay-corrected total activity at time t. The resulting time–activity data are shown in Supplemental Table 3.

The software tool ROVER (ABX advanced biochemical compounds) was used to define the volumes of interest (VOIs)—that is, the target organs—to determine the activity as well as the respective volume. A rigid image registration of the PET and CT data was done with ROVER, visually checked and manually corrected when needed. Relevant organs including brain, gallbladder, large intestine, small intestine, stomach, heart wall, kidneys, liver, lungs, pancreas, red marrow, spleen, testes, thyroid, and urinary bladder were manually defined (VOIs) as shown in Figure 1 (piglets) or Figure 2 (humans), and the respective activity values were extracted. The %ID was calculated using Equation 1.

A calibration of the image data was performed as described in the supplemental material.

WB Dosimetry

To make the investigations of 3 species comparable to each other, the hermaphroditic adult male model (the 73.7-kg standard man) was used for animal as well as human dosimetry calculations. This was possible because of the scaling of animal biokinetic data (%ID values and time scales) from mice and piglets to human anatomy before input into OLINDA/EXM. The scaling is described in detail in the supplemental material.

The OLINDA/EXM program outputs the mean doses to humans to 25 target organs, and the ED was calculated using the tissue weighting factors provided in ICRP publication 103 (11).
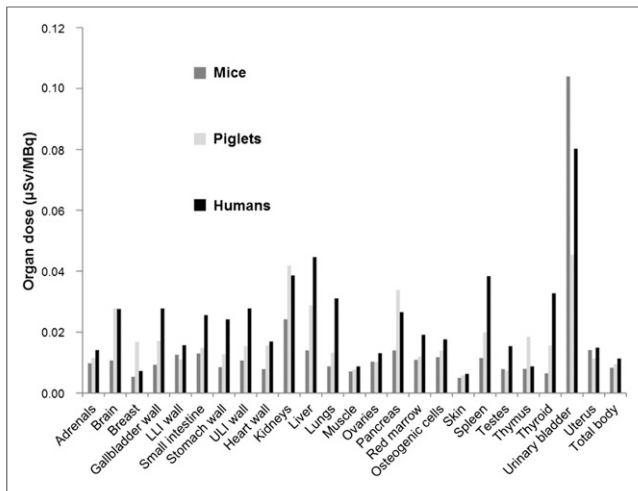
FIGURE 6. Organ doses of all investigated species. Calculated ODs are summarized and visualized in this chart for examined species. Liver, kidneys, and urinary bladder in all 3 species uniformly take up high amount of activity. Dose values of spleen, thyroid, and skin are highly spread. LLI = lower large intestine; ULI = upper large intestine.

Dosimetry of Urinary Bladder

The dosimetry of the urinary bladder requires special consideration. This organ accumulated the highest amounts of the radiotracer, with the activity in the urinary bladder contents therefore contributing relatively high doses to the bladder wall as well as nearby organs.

The mice data were obtained by counting the dissected urinary bladder together with the collected urine at each time point in the γ counter and used to create the time–activity curve for that organ. Because there was no micturition during the imaging sessions of the piglets, we extracted the activity data by creating a VOI inside the organ at different time points. To validate the accuracy of the measured activity, the urine was collected and counted in 1 mL samples after the piglets were sacrificed. To verify, the data were decay-corrected to the micturition time and compared with the urinary bladder VOI of the last scan. As shown in the scan protocol (Supplemental Table 2), the human volunteers left the PET/CT table 4 times for collection of urine. One-milliliter samples of the collected urine were assayed in a γ counter and decay-corrected to the micturition time. The total excreted activity is obtained by multiplying the measured whole volume of voided urine with the counted activity concentration. Dividing this result with the administered activity and multiplying by 100 yields the %ID. Because the dynamic voiding-bladder model (10) assumes the complete

emptying of the urinary bladder, it is not suitable for this investigation. Instead, the trapezoidal-integration equation

$$\widetilde{\%ID}_{urinary\ bladder} = \frac{1}{2}\sum_{i=1}^{n-1}(\%ID_i + \%ID_{i+1})(t_{i+1} - t_i), \quad \text{Eq. 2}$$

was used to determine the cumulated activity in the urinary bladder ($\widetilde{\%ID}_{urinary\ bladder}$), where $\%ID_i$ is the activity value at a time point t_i, respectively. Using the image information and the counted urine, we created a graph showing the %ID and the voided volume of urine over time (Fig. 3). The relationship shown in this chart highlights that the urinary bladder is not completely emptied, so that the voiding-bladder model (12) for dose calculation is not optimal.

Application of the trapezoid equation (integrate the surface under the curve) yields the cumulative activity $\widetilde{\%ID}_{urinary\ bladder}$ and the number of disintegrations in the urinary bladder for input of the kinetic data in OLINDA.

RESULTS

After an intravenous injection of $(-)$-^{18}F-flubatine, no study drug–related adverse pharmacologic effects occurred during the investigation time. Urine and blood tests showed normal results. Representative $(-)$-^{18}F-flubatine PET images of piglets (80 min after injection) and humans (100 min after injection) are presented in Figures 1 and 2, respectively, in coronal, sagittal, and transverse views. The brain (target organ), liver, kidneys, and urinary bladder can clearly be identified. These figures also illustrate the delineated VOIs, created after coregistration with the CT images, of the respective subject in ROVER. The WB PET series shown in Figure 4 clarifies the filling and emptying of the urinary bladder as well as the high activities in the liver during the first hour after injection and the subsequent clearance. The resulting activity values are presented in Supplemental Table 3. Representative time–activity curves and the respective exponential fit functions are shown in Figure 5 for 6 organs. The organ doses based on the animal data were calculated using the adult male model (73.7-kg hermaphroditic standard man) as implemented in OLINDA. A comparison of the mouse data to the human data is therefore possible as follows.

Because of the clearance circumstances of this tracer as observed during the first hour after injection, a high uptake in the liver and urinary bladder can be identified. As a result, the organ doses in all 3 species were found to be highest in the urinary bladder wall (104.0, 45.5 ± 19.4, and 80.2 ± 37.8 μSv/MBq for mice, piglets, and humans, respectively) and the kidneys

TABLE 4
Comparison of ED for Different PET Tracers Based on Preclinical and Clinical Dosimetry Studies

Tracer	Target organ	Clinical (μSv/MBq)	Preclinical (μSv/MBq)	Deviation (%)	Reference
$(-)$-^{18}F-flubatine	Brain	23.4	12.5 (mouse)	44.0	This study
			14.7 (piglet)	34.0	
^{18}F-RGD-K5	Cancer imaging	31.0	22.2 (monkey)	28.4	(20)
^{18}F-BMS747158	Myocardial imaging	19.0	15 (monkey)	21.1	(21,22)
^{18}F-FEDAA1106	Evaluation of neuroinflammatory diseases	36.0	23.5 (mouse)	34.7	(23)
[11]C-choline	Oncologic	4.4	2.8 (rat)	36.0	(24)
[11]C-DASB	Brain	7.0	6.2 (monkey)	11.4	(25,26)
[11]C-telmisartan	Liver	4.2	3.7 (rat)	13.1	(27)

(24.2, 41.8 ± 7.3, and 38.6 ± 5.1 μSv/MBq for mice, piglets, and humans, respectively). Tables 1–3 show the mean OD as well as ED values of 25 organs in the 3 investigated species. In this study, the calculated EDs to humans based on mouse, piglet, and human data were 12.5, 14.7 ± 0.7, and 23.4 ± 0.4 μSv/MBq, respectively. For an administration of 300 MBq in a brain study, the corresponding ED estimates to humans are 3.75, 4.41, and 7.02 mSv.

DISCUSSION

The values (%ID/organ, 15 min after injection) of the liver (mice, 8.7; piglets, 15.9 ± 6.9; humans, 18.9 ± 2.4) and kidneys (mice, 4.6; piglets, 4.2 ± 2.3; humans, 4.6 ± 0.7) were significantly higher than those of the remaining organs but decreased because of the clearance in these organs. At the end of the respective measurement, the values decreased significantly for the liver (mice, 0.05 ± 0.02; piglets, 5.4 ± 2.1; humans, 8.4 ± 1.2) and kidneys (mice, 0.01 ± 0.003; piglets, 1.4 ± 0.3; humans, 1.4 ± 0.3). These organs are the most highly exposed in all investigated species, with organ doses comparable to those of other ^{18}F-labeled tracers (e.g., ^{18}F-mefway, ^{18}F-nifene) (13,14) as well as to the ^{11}C-labeled ^{11}C-WAY (15). Figure 6 shows a summary of all ODs for the 3 investigated species. Information on the comparison to tracers that target similar receptors can be found in the supplemental material.

To achieve an adequate image quality, the German Federal Office for Radiation Protection (Bundesamt für Strahlenschutz) proposes for ^{18}F-labeled tracers the administration of between 200 MBq (brain imaging) and 350 MBq (WB PET imaging for tumor detection) to an adult human (16). After the injection of 300 MBq of (−)-^{18}F-flubatine, for instance, this will result in an effective dose of about 3.75, 4.41, and 7.02 mSv (mouse, piglet, and human, respectively) based on the data as presented in this work.

In general, the dosimetry results and the deviation of preclinical from clinical phase data is within the range of those of other ^{18}F-labeled tracers as shown in Table 4. As described in the "Methods" section, a scaling of the time and activity data to the human entity primarily can compensate for the faster metabolism of small animals but not for the differences in tracer distribution due to different species. For a prediction of further preclinical studies and the respective dosimetry, the results of this study suggest that there is an underestimation of the ED to humans as assessed by preclinical studies of about 40% when scaled biokinetic data from preclinical studies are used with the hermaphrodite adult male model. Given that the sought-after ED to humans is 100%, the correction should be done with the rule:

$$ED_{hum} = \frac{ED_{hum_{pre}}}{k}, \qquad \text{Eq. 3}$$

where the ED_{hum} is the ED to humans corrected for underestimation by preclinical assessment, the $ED_{hum_{pre}}$ is the ED to humans assessed from preclinical data scaled to human anatomy, and k is the correction factor (e.g., 0.6 given an underestimation of 40%).

Comparing our results with the reference doses given by ICRP publications 53, 80, and 106 (17), we found that (−)-^{18}F-flubatine caused a radiation risk in the same low order of magnitude as, for instance, ^{18}F-FDG (19.0 μSv/MBq). An explanation for a similar dosimetry result of different ^{18}F-labeled tracers is given by Bottlaender et al. (18). As stated there, the contribution to the residence time (normalized cumulated activity) in an organ is mostly affected by the short half-life of ^{18}F rather than by the different biologic half-lives of the active molecules. This statement emphasizes that the preclinical underestimation of the effective dose to humans of 40% would be applicable not only for tracers similar to flubatine but also for other ^{18}F-labeled substances (19).

CONCLUSION

As has been demonstrated for other PET radiotracers, preclinical (i.e., animal-derived) dosimetry underestimates the ED to humans, in the current case of (−)-^{18}F-flubatine by 34%–44%.

DISCLOSURE

ACKNOWLEDGMENT

REFERENCES

1. Quik M, Wonnacott S. α6β2* and α4β2* nicotinic acetylcholine receptors as drug targets for Parkinson's disease. *Pharmacol Rev.* 2011;63:938–966.
2. Brašić JR, Cascella N, Kumar A, et al. Positron emission tomography experience with 2-^{18}F-fluoro-3-(2(S)-azetidinylmethoxy)pyridine (2-^{18}F-fa) in the living human brain of smokers with paranoid schizophrenia. *Synapse.* 2012;66:352–368.
3. Wu J, Ishikawa M, Zhang J, Hashimoto K. Brain imaging of nicotinic receptors in Alzheimer's disease. *Int J Alzheimers Dis.* 2010;2010:548913.
4. Fischer S, Hiller A, Smits R, et al. Radiosynthesis of racemic and enantiomerically pure (−)-[18F]flubatine: a promising PET radiotracer for neuroimaging of α4β2 nicotinic acetylcholine receptors. *Appl Radiat Isot.* 2013;74:128–136.
5. Brust P, Patt JT, Deuther-Conrad W, et al. In vivo measurement of nicotinic acetylcholine receptors with [18F]norchloro-fluoro-homoepibatidine. *Synapse.* 2008;62:205–218.
6. McParland BJ. *Nuclear Medicine Radiation Dosimetry: Advanced Theoretical Principles.* London, U.K.: Springer; 2010:456–460.
7. Deuther-Conrad W, Patt JT, Feuerbach D, Wegner F, Brust P, Steinbach J. Norchloro-fluoro-homoepibatidine: specificity to neuronal nicotinic acetylcholine receptor subtypes in vitro. *Farmaco.* 2004;59:785–792.
8. Patt M, Schildan A, Habermann B, et al. Fully automated radiosynthesis of both enantiomers of [18F]flubatine under GMP conditions for human application. *Appl Radiat Isot.* 2013;80:7–11.
9. Lindstedt SL, Schaeffer PJ. Use of allometry in predicting anatomical and physiological parameters of mammals. *Lab Anim.* 2002;36:1–19.

10. Thomas SR, Stabin MG, Chen CT, Samaratunga RC. MIRD pamphlet no. 14 revised: a dynamic urinary bladder model for radiation dose calculations. Task Group of the MIRD Committee. *J Nucl Med.* 1999;40:102S–123S.

11. The 2007 recommendations of the International Commission of Radiological Protection: ICRP publication 103. *Ann ICRP.* 2007;37:1–332.

12. Stabin MG. *Fundamentals of Nuclear Medicine Dosimetry.* New York, NY: Springer; 2008:130–137.

13. Constantinescu CC, Sevrioukov E, Garcia A, Pan M-L, Mukherjee J. Evaluation of [18F]mefway biodistribution and dosimetry based on whole-body PET imaging of mice. *Mol Imaging Biol.* 2013;15:222–229.

14. Constantinescu CC, Garcia A, Mirbolooki MR, Pan M-L, Mukherjee J. Evaluation of [18F]Nifene biodistribution and dosimetry based on whole-body PET imaging of mice. *Nucl Med Biol.* 2013;40:289–294.

15. Parsey RV, Belanger MJ, Sullivan GM, et al. Biodistribution and radiation dosimetry of 11C-WAY100, 635 in humans. *J Nucl Med.* 2005;46:614–619.

16. Federal Office for Radiation Protection. Notice of the updated diagnostic reference values for nuclear medicine investigations. *Federal Ministry of Justice, Federal Gazette (BAnz).* B5, October 19, 2012:1–6.

17. Valentin DJ. Recalculated dose data for 19 frequently used radiopharmaceuticals from ICRP Publication 53. *Ann ICRP.* 1998;28:47–83.

18. Bottlaender M, Valette H, Roumenov D, et al. Biodistribution and radiation dosimetry of 18F-fluoro-A-85380 in healthy volunteers. *J Nucl Med.* 2003;44:596–601.

19. Zanotti-Fregonara P, Lammertsma A, Innis R. Suggested pathway to assess radiation safety of 18F-labeled PET tracers for first-in-human studies. *Eur J Nucl Med Mol Imaging.* 2013;40:1781–1783.

20. Doss M, Kolb HC, Zhang JJ, et al. Biodistribution and radiation dosimetry of the integrin marker 18F-RGD-K5 determined from whole-body PET/CT in monkeys and humans. *J Nucl Med.* 2012;53:787–795.

21. Maddahi J, Czernin J, Lazewatsky J, et al. Phase I, first-in-human study of BMS747158, a novel 18F-labeled tracer for myocardial perfusion PET: dosimetry, biodistribution, safety, and imaging characteristics after a single injection at rest. *J Nucl Med.* 2011;52:1490–1498.

22. Lazewatsky J, Azure M, Guaraldi M, et al. Dosimetry of BMS747158, a novel 18F labeled tracer for myocardial perfusion imaging, in nonhuman primates at rest [abstract]. *J Nucl Med.* 2008;49(suppl 1):15P.

23. Takano A, Gulyás B, Varrone A, et al. Biodistribution and radiation dosimetry of the 18 kDa translocator protein (TSPO) radioligand [18F]FEDAA1106: a human whole-body PET study. *Eur J Nucl Med Mol Imaging.* 2011;38:2058–2065.

24. Tolvanen T, Yli-Kerttula T, Ujula T, et al. Biodistribution and radiation dosimetry of [11C]choline: a comparison between rat and human data. *Eur J Nucl Med Mol Imaging.* 2010;37:874–883.

25. Tipre DN, Fujita M, Chin FT, et al. Whole-body biodistribution and radiation dosimetry estimates for the PET dopamine transporter probe 18F-FECNT in nonhuman primates. *Nucl Med Commun.* 2004;25:737–742.

26. Lu JQ, Ichise M, Liow JS, Ghose S, Vines D, Innis RB. Biodistribution and radiation dosimetry of the serotonin transporter ligand 11C-DASB determined from human whole-body PET. *J Nucl Med.* 2004;45:1555–1559.

27. Shimizu K, Takashima T, Yamane T, et al. Whole-body distribution and radiation dosimetry of [11C]telmisartan as a biomarker for hepatic organic anion transporting polypeptide (OATP) 1B3. *Nucl Med Biol.* 2012;39:847–853.